resources

Article

Integration of Well Logging and Remote Sensing Data for Detecting Potential Geothermal Sites along the Gulf of Suez, Egypt

Amr S. Fahil [1,2], Eman Ghoneim [1,*], Mohamed A. Noweir [2] and Alaa Masoud [2]

1 Department of Earth and Ocean Sciences, University of North Carolina Wilmington, 601 South College Road, Wilmington, NC 28403-5944, USA; amr_shaban@science.tanta.edu.eg

2 Geology Department, Faculty of Science, Tanta University, Tanta 31527, Egypt; atefnoweir@yahoo.com (M.A.N.); alaamasoud09@live.com (A.M.)

* Correspondence: ghoneime@uncw.edu; Tel.: +1-910-962-2795

Received: 7 August 2020; Accepted: 2 September 2020; Published: 4 September 2020

Abstract: The Gulf of Suez area is one of the most favorable regions in Egypt for geothermal exploitation since it hosts an evident cluster of superficial thermal springs. Some of these thermal springs include Hammam Musa, Hammam Faraun, Sudr, Ayn Musa and Ain Sokhna, which are characterized by high temperatures ranging between 35 °C to 86.66 °C. It is this feature that makes the Gulf of Suez locality sufficient for geothermal power production. Corrected bottom hole temperature (BHT) data from 197 oil wells situated onshore and offshore of the Gulf of Suez were utilized for the present research. The results indicated that the study area has a geothermal gradient ranging from 24.9 to 86.66 °C/km, a heat flow ranging from 31 to 127.2 m W k^{-1}, a thermal conductivity of 2.6–3.2 W m^{-1} k^{-1}, and an amplitude temperature varying from 49.48 °C to 157.8 °C. The derived geothermal and geological layers were used together with the remote sensing thermal infrared and topographic data, to map relevant physiographic variables including surface elevation, fractures density, drainage density, nighttime land surface temperature and major lithological units. The nine produced variables were integrated in GIS to model the geothermal potential map (GTP) for the Gulf of Suez region. The model identifies the northeastern and the southwestern areas as equally two sites for high geothermal potential. Findings of this study demonstrate that integration of well logging and space data with the adopted geospatial techniques is a practical method for geothermal prospecting in similarly geologic and tectonic setting in Egypt and East Africa.

Keywords: well logging data; bottom-hole temperature (BHT); Landsat thermal infrared; DEM; fractures density; stream density; GIS

1. Introduction

Nowadays, Egypt is witnessing unprecedent expansion of domestic, urban and economic expansion [1]. This expansion puts a considerable stress on the current energy resources of Egypt, in particular, electricity resources. It is projected that the country consumption from electricity will be increasing at a rate of 1500–2000 MW per year. Thus, the search for new energy resources, such as geothermal energy, became of a vital importance to cope with the rapid economic and urban growth in Egypt.

African and Arabian countries have an abundance of geothermal energy resources that are not currently utilized for electrical resource delivery. The development of the geothermal systems in these countries is relatively recent and was initiated during the separation of the Arabian–Nubian Shield (ANS) between 31 and 15 Ma [2–6]. The breakup of the ANS activated large-scale volcanic and tectonic activities over the Arabian shield including the present-day countries of Yemen, Egypt, Eritrea, Djibouti, Ethiopia and Kenya [2–5]. The expanded region surrounding the Red Sea continues to be vastly active and dynamic with tectonic events. These energetic events have historically resulted in the expansion and proliferation of geothermal systems in the region.

In Egypt, the earliest magmatic activity was informed from Zabargad Island (~6.6–1.3 Ma) [7,8] with magmatic activity being characterized by basalt flows and dike swarms [9,10]. All the geothermal systems in the African and Arabian countries are directly related to the volcanic and magmatic activity associated with the rifting of the Red Sea [11,12]. From the arid Sahara to the extensive Nile River, Egypt has an abundance of natural diversity. Located within the uppermost northeast quadrant of Africa, Egypt links the continent with the Middle East by bordering with the southern Levant region. To the east, Egypt borders the Red Sea. This adjacency to the Red Sea Rift, a scientifically classified divergent plate boundary with a spreading center between the African and Arabian plates [13], provides a distinct tectonic setting which positions Egypt to have substantial geothermal resources [14]. The eastern and western coasts of the Gulf of Suez within the northwest Red Sea include a cluster of hot springs with a range of characteristic temperature variations (e.g., Hammam Musa, Hammam Faraun, Sudr, Ayn Musa and Ain Sokhna). These hot spring regions are the most promising for geothermal development [12] (Figure 1). The hot spring of Hammam Faraun contains high geothermal variables including a measured heat flow of 127.2 m W k^{-1}. This value is about three times the average values in the eastern part of Egypt [15]. El-Nouby [16] analyzed the potassium deposits in the Middle Miocene Evaporites in the Gulf of Suez and determined that the radioactivity and the isothermal maps, which represent patterns of constant or equal temperature, have similar alignments, which are congruent with the main structure trends of the area. While previous studies have provided localized detail information, it is noted that geothermal studies on the periphery of the region were sparse which limits the characterization of the regional supply of the geothermal potential distributed across the study area.

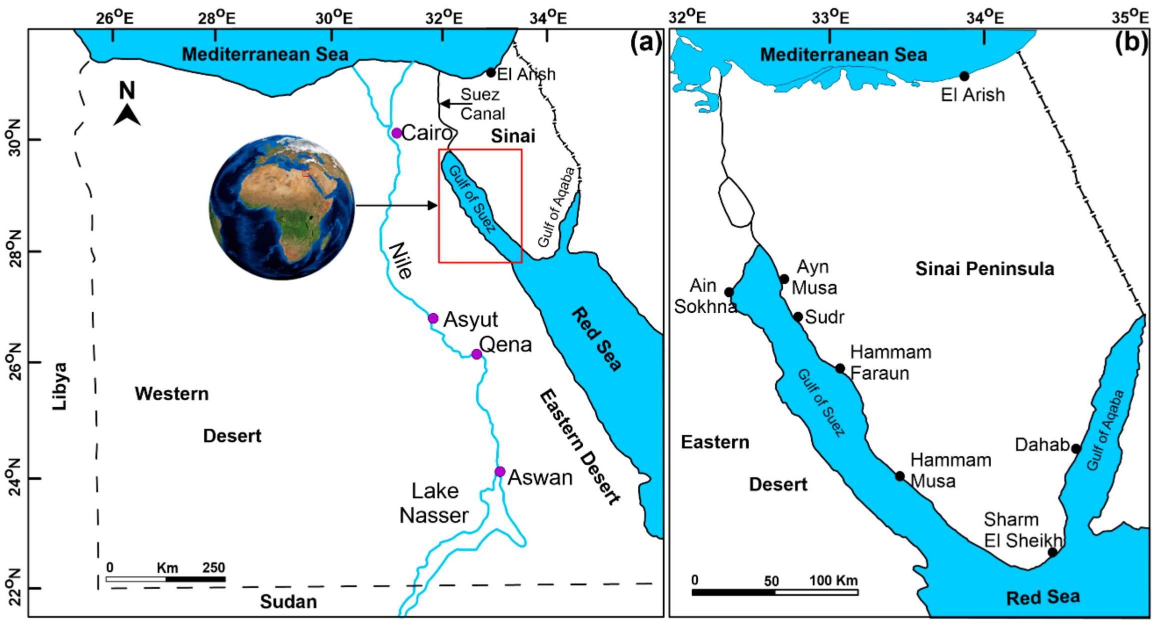

Figure 1. (**a**) Shows the location of the study area marked by the red box, (**b**) position of the thermal springs, along the Gulf of Suez rift.

The development of a sustainable geothermal resource relies heavily upon integrating the geology and dominating structures with the geothermal properties of the potential reservoir rocks including reservoir temperatures, permeability, and thermal conductivity. Accurate characterization of fractures is crucial to the formulation of proper management plans for geothermal energy development. The present research aims to build a geologic-geothermal model to enhance the geothermal potential evaluation and exploration of future resources. The primary objective of this study is to develop an approach that can be used to evaluate geological, structural and topographical data that are related to the geothermal resources of the Gulf of Suez area and its impacts. To derive this information, this research incorporated remote sensing and GIS techniques with field data measurements (onshore and offshore wells) to locate and evaluate geothermal development potential. Ultimately, this approach aims to provide guidance for the determination and identification of new localities for geothermal energy resources and delivery infrastructure. Utilizing the general trends and spatial distribution of potentially suitable areas for geothermal power plant and electricity production, valuable information can be provided to community planners and developers to inform land use, urban development, and electrical resource delivery decisions.

2. Geological and Tectonic Setting

The initiation and evolution of the Red Sea Rift and the transition from a continental to an oceanic rift occurs in the Red Sea near the Gulf of Aden and spreads north into the Sinai province, leading to the formation of the Gulf of Suez rift (Figure 2) [17,18]. As a result of extensional forces formed by a rising mantle plume beneath the Afar region where an upwelling mantle plume is uplifting the region, the Arabian Shield rotated anti-clockwise over a transform fault near the Gulf of Aqaba. As a result, the Red Sea Rift could not penetrate the Precambrian shield south of Sinai. Consequently, the rift axis stopped at the Gulf of Suez (termed as a failed arm) [3,8,19–23]. The geology of the area under study ranges from pre-Cambrian basement rocks to the Holocene Quaternary deposits (Figure 3) [24–27].

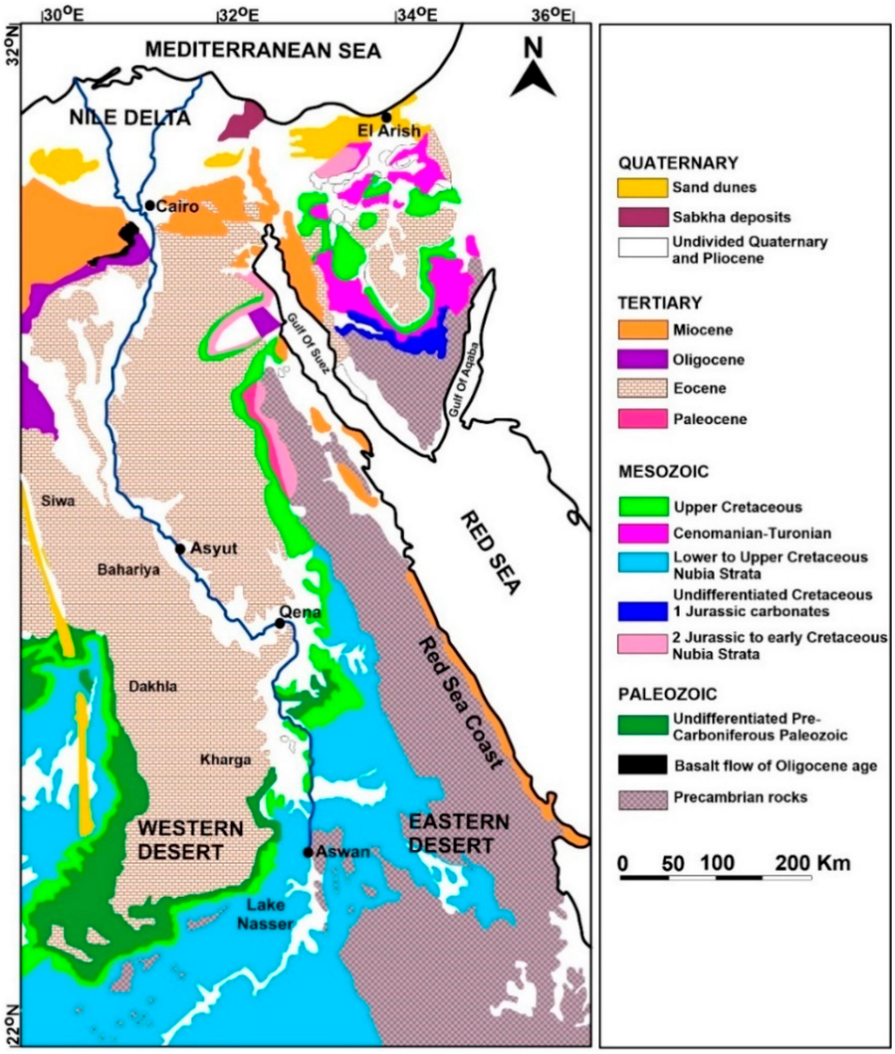

Figure 2. Geological map of Egypt modified after [17,18].

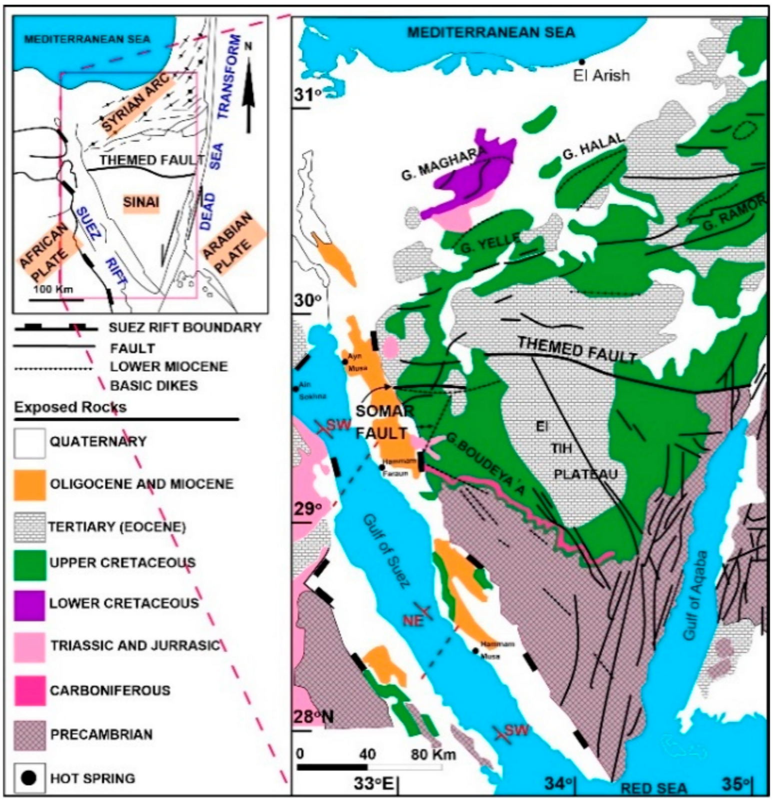

Figure 3. Shows the geology and structural setting of Sinai Peninsula. Modified after [24–27].

The Gulf of Suez is located at the northwestern end of the Red Sea, to the west of the Sinai Peninsula. It stretches 300 km (190 mi) north in a NW-SE trending rift that is divided into three parts: the northern, central and southern segments. The northern part of the Gulf dips to SW; the central part dips to the NE, and the southern segment dips to the SW [28]. The structure of the Gulf of Suez rift is controlled by extensional normal faults and rotational block faulting which is considered to be a mode of structural evolution in extensional tectonic events and a result of tectonic plates stretching apart. The crests of these plates represent the main target for oil and hydrocarbon exploration. The pattern swarms of extensional faults consist of two major groups of trends. The first rupture is linear with longitudinal stripes positioned parallel to the axis of the Gulf of Suez rift which was generated an extensional system during Neogene time. The second rupture is N–S to NE–SW trending with transverse faults containing inactive discontinuities in the pre-Cambrian basement rock [20]. The stratigraphic succession of the Gulf of Suez, modified after [29], is illustrated in Figure 4 to show the dominant geological formations and thickness.

Intensive structural and tectonic events have been present in this region from the Cretaceous to Pleistocene. Maximum activity of faulting and subsidence is dated to have occurred during the latter stages of Oligocene while more present-day activity consists of significant hot spring structures. Many of these active hot springs which have been attributed to the Red Sea and Gulf of Suez divergent rifts are located along the eastern and western coastal margins of the Gulf of Suez [30]. The relationship of the geothermal feature localities and the physical features of the Gulf of Suez have been accompanying with the pre-Miocene break [31]. Features associated with high temperatures are reflective of more shallow blocks whereas cooler temperatures are linked with more deep pre-Miocene blocks [32]. The main depressions located along the Gulf of Suez rift axis are related to a gradient of high thermal measurements on the order of 20 °F per 30 m, which is attributed to the convective flux of high temperature mantel flowing upwards to the thin crust surface [33]. To the upper east of Egypt's mainland lies the arid Sinai Peninsula with an area of 60,000 square kilometers. It is situated between the Gulf of Suez on the west and the Gulf of Aqaba on the east. The Mediterranean Sea borders the northern expanse of the Sinai while the southern triangular tip shares a boundary with the Red Sea. Because of its positioning and geologic formation, Sinai contains geologic and geomorphological features that are characteristically non congruent with the surrounding land masses.

The Upper Peninsula is comprised of low elevation alluvial expanses interspersed with uplifted Mesozoic domes and anticlines of the Syrian Arc (Figure 3). As a result of sinking processes along Tertiary fault structures, these Syrian arc features are located below the Quaternary deposits in close proximity to the Mediterranean Sea [30]. The mid-section of the Sinai is comprised of a diversity of geologic settings while containing both Mesozoic and Tertiary sediments. The arid southern tip contains significant mountainous topography with an elevation range of 2450 m and is comprised of pre-Cambrian basement rocks [34].

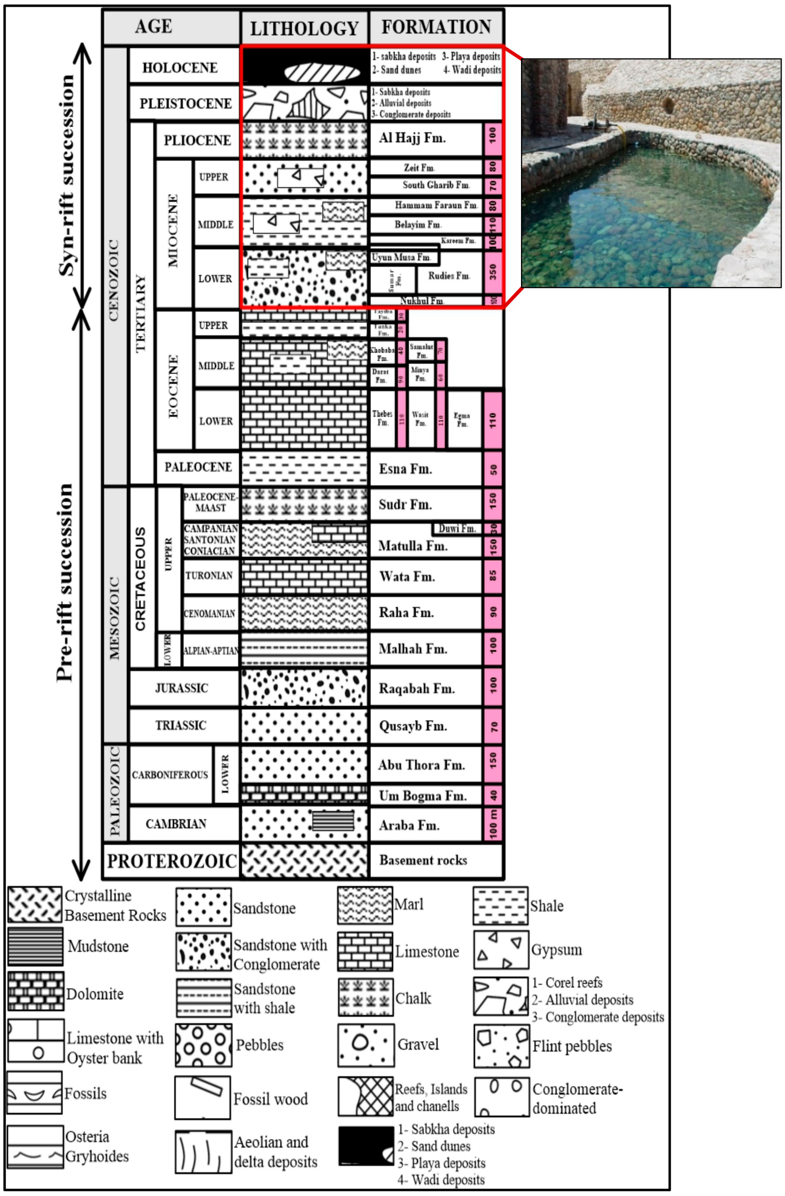

Figure 4. The stratigraphic succession of the Gulf of Suez, showing dominant geological formation and thickness (modified after [29]). Ayn Musa stratigraphic succession is marked by a red box with a photo showing Ayn Musa (Source: [35]).

3. Materials and Methods

The workflow for this study consists of two main procedures, first: variable extraction and mapping using the compiled well logging, geological and remote sensing data products, and second: geothermal potentiality analysis and modelling. A simplified workflow of the data and methods used is outlined in Figure 5.

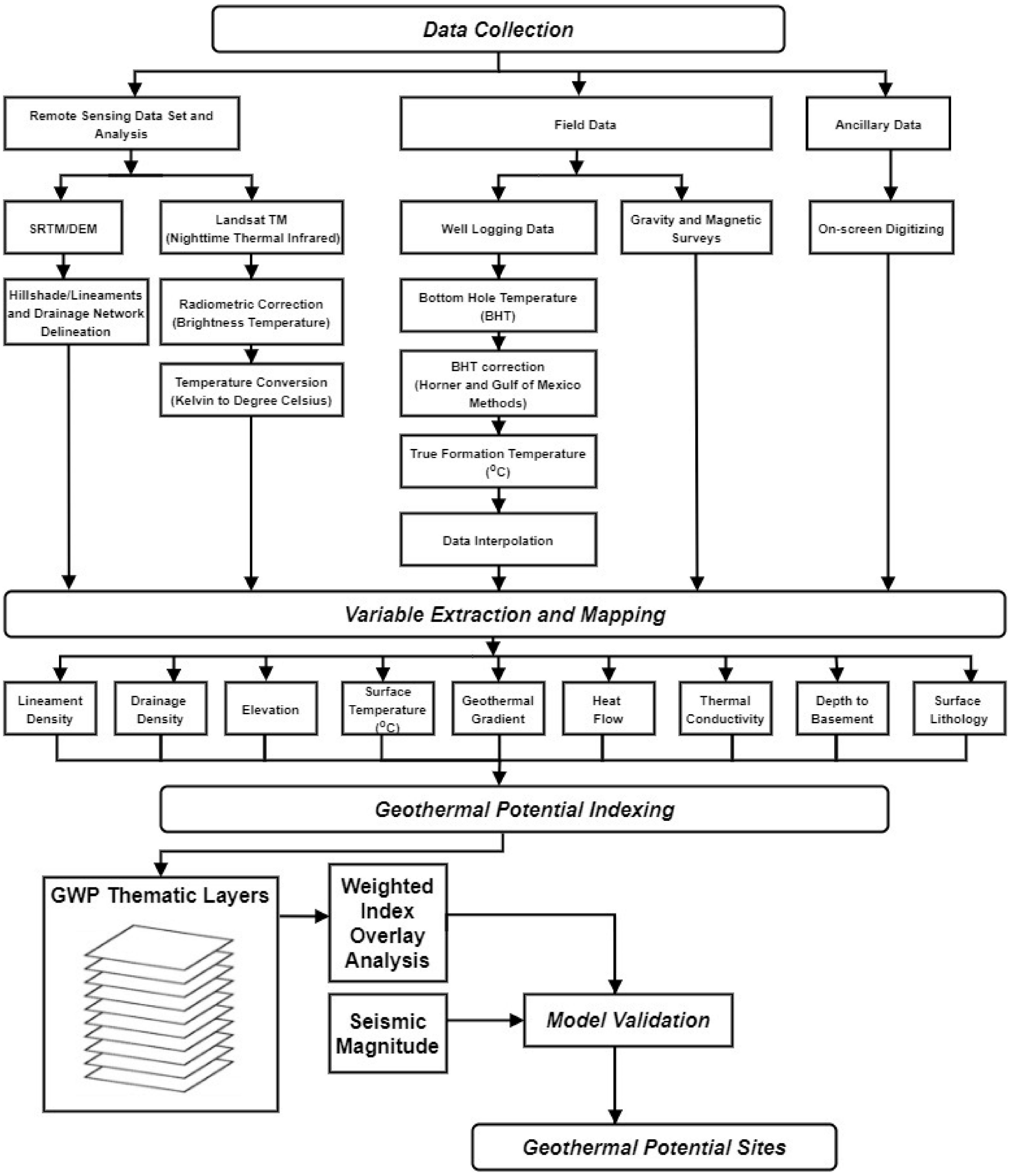

Figure 5. Simplified project workflow.

3.1. Well Logging Data

Geothermal analysis was conducted using the well logging data from 197 deep oil wells (n = 160 onshore and n = 37 offshore) along the Gulf of Suez region, with depths ranging from 158.3 to 4223 m. The bottom-hole temperatures (BHT) of well data were collected by the Egyptian General Petroleum Company (EGPC), the Gulf of Suez Petroleum Company (GUPCO), and British Petroleum Company (BPC). BHT, commonly used in geothermal studies, remains the most abundant and readily available source for subsurface temperature information. These temperature measurements are collected at the time of active drilling or shortly after drilling circulation has ceased. Due to the convective cooling effect of fluid introduction in the mechanical drilling process, the temperatures measured with this procedure are reduced in comparison to their baseline temperatures [36–38]. After the drilling process concludes and no further cooling fluids are added, the borehole steadily returns to a less altered formation temperature. The temperature measurements collected are reflective of the equilibrium formed between the thermally cool drill fluid and the high temperature of the underlying formation—notably, raw BHT measurements reflect temperatures that are cooler than actual formation temperatures [36,37,39,40]. Corrections for the raw BHT can be made when the BHT measurement, time since circulation, and/or depth of measurement are known.

In order to address the temperature differentials between the logged BHT measurements and the real formation temperature, various correction methods have been utilized [36–43]. In this study, BHT data were corrected by applying the widely used Horner, and Gulf of Mexico correction methods to obtain the actual formation temperatures. The Horner method (1951) [36], is suitable if a series of BHT data from sequential well logging efforts is accessible. This method is limited by the reliance upon assumptions which are warranted by the scarcity of time consumptive and resource prohibitive documentation of drilling procedures. One such parameter includes the actual length of time mud is circulated in the well. The Horner correction utilizes the timing of events in the drilling process based on the presence of a linear heat source calculation. The Horner correction was calculated using the following equation:

$$T_{eq} = T_{BHT} = Alog + \left(1 + \frac{T}{t}\right) \quad (1)$$

where: A is temperature measured, T_{eq} (°C) is the corrected temperature at equilibrium, T (h) is the cooling duration (assumed to be 10 h as circulation durations less than this threshold are deemed to have a negligible effect), t (h) is the time since circulation, which is the interval between the drilling fluid cessation and well logging initiation, and T_{BHT} (°C) is the bottom hole temperature measurement.

The second method, by Waples et al., 2004 [37], is the Gulf of Mexico correction method. This method was developed to correct log-derived temperatures. The method made comparative calculations utilizing log temperatures and drill stem test temperatures of deep well (3500–6500 m) samples in a Gulf of Mexico site, Gulf of Campeche. The correction is strongly linked to the time duration following mud circulation cessation (TSC), and secondarily on depth. The Gulf of Mexico subsurface temperatures (°C) corrections were calculated using the following equation:

$$T_{true} = T_{surface} + f * \left(T_{measured} - T_{surface}\right) - 0.001391(Z - 4498) \quad (2)$$

where $T_{measured}$ (°C) is log temperature measurement, Z (m) is depth below the seafloor surface, $T_{surface}$ is the annual mean temperature at the seafloor or land surface interface, 26.7 °C, and f correction factor, which is a function of time since circulation cessation derived using Equation (3):

$$f = [-0.1462 * In\ (T_{SC}) + 1.699]/0.572 * Z^{0.075} \quad (3)$$

Table 1, shows the similarity of the derived values from the above two methods, thus supporting the corrected formation temperature outcomes. Corrected formation temperatures were further used to generate a geothermal gradient for each well within the study area based on an average yearly surface temperature of 26.7 °C as incorporated in Equation (3) [44].

Table 1. Bottom-Hole Temperatures using the Gulf of Mexico and Horner BHT Correction Methods.

Well Name	Latitude	Longitude	Depth (m)	Gulf of Mexico		Horner	
				(°F)	(°C)	(°F)	(°C)
GS-327	28.20 N	33.57 E	2542	243.74	117.6	250.24	121.2
GS-346	28.09 N	33.55 E	3033	247.92	119.9	249.76	120.9
GS-277	28.41 N	33.30 E	4171	318.69	159.2	358.74	181.5
GS-160	28.94 N	33.99 E	4226	328.65	164.8	312.60	155.8
GS-316	28.23 N	33.50 E	3825	274.15	134.5	259.84	126.5
Amal-10-A	28.34 N	33.34 E	2600	101.52	38.6	91.91	33.2
SB-296	28.30 N	33.44 E	4152	268.9	131.6	267.43	130.7
SB-367	28.03 N	33.72 E	3418	276.35	135.7	317.56	158.6
GS-325	28.21 N	33.44 E	3184	272.82	133.7	294.93	146.1
SB-366	28.02 N	33.66 E	3687	312.46	155.8	330.81	166

The geothermal gradient is the change of temperature ΔT (°C) with depth ΔZ (meters) [45]. The geothermal temperature gradient was calculated using Equation (4):

$$GG = \frac{T - Ts}{Z} = \frac{dT}{dZ} \tag{4}$$

where GG (°C/m) is the geothermal gradient, T (°C) is the formation temperature (BHT), Ts (26.7 °C) is the mean annual surface temperature and Z (m) is the total depth. An additional temperature parameter of heat flow was calculated for the study area. Heat flow quantifies the transfer of heat energy from the Earth's core to the Earth's surface. This heat results from two primary sources including the heat that originates and is dissipated from the Earth's core and the heat that is produced from radioactive decay within the Earth's crust [45]. The values for the Heat flow were determined by combining sets of temperature gradients and thermal conductivity data using Equation (5):

$$Q = K\,(dT/dZ) \tag{5}$$

where Q is heat flow (m W k^{-1}), K (W m^{-1} K^{-1}) is thermal conductivity, dT (°C) is the temperature change in a depth interval of dZ (m). Thermal Conductivity is a measure of conductive heat transfer through a material. This conductivity varies for individual rocks and fluids based on physical composition and structural properties of the material [46]. The thermal conductivity across the study area were determined using Equation (6):

$$K = \frac{Q}{A\Delta T} \tag{6}$$

where K (W m^{-1} K^{-1}) is thermal conductivity, Q (m W k^{-1}) is heat flow, A (m^2) is the area of the body, ΔT is difference in temperature.

The depth to basement metric (also referred to as the depth to crystalline basement) was the fourth variable to be extracted for the area. The depth data were obtained from the most recent well data drilled to the pre-Cambrian basement by Egyptian General Petroleum Corporation (EGPC 2000) and extracted from gravity and magnetic surveys. The depth to basement is typically defined as the depth to the top surface of igneous or metamorphic rocks which are either loose sediments or sedimentary rocks. Impedance contrasts are often observed at the interface between these rock types.

The geothermal gradient, heat flow, thermal conductivity and depth to basement points data, derived from the corrected onshore n = 37 well logging data, were interpolated using the inverse distance weighting (IDW) method in ArcGIS to generate a continuous raster layer across the study area for inclusion in the GIS-based geothermal potential model (Figure 6). This interpolation method is simply used to provide an estimation of values at unsampled locations derived from measurements of measured values of surrounding points and the distance between those points.

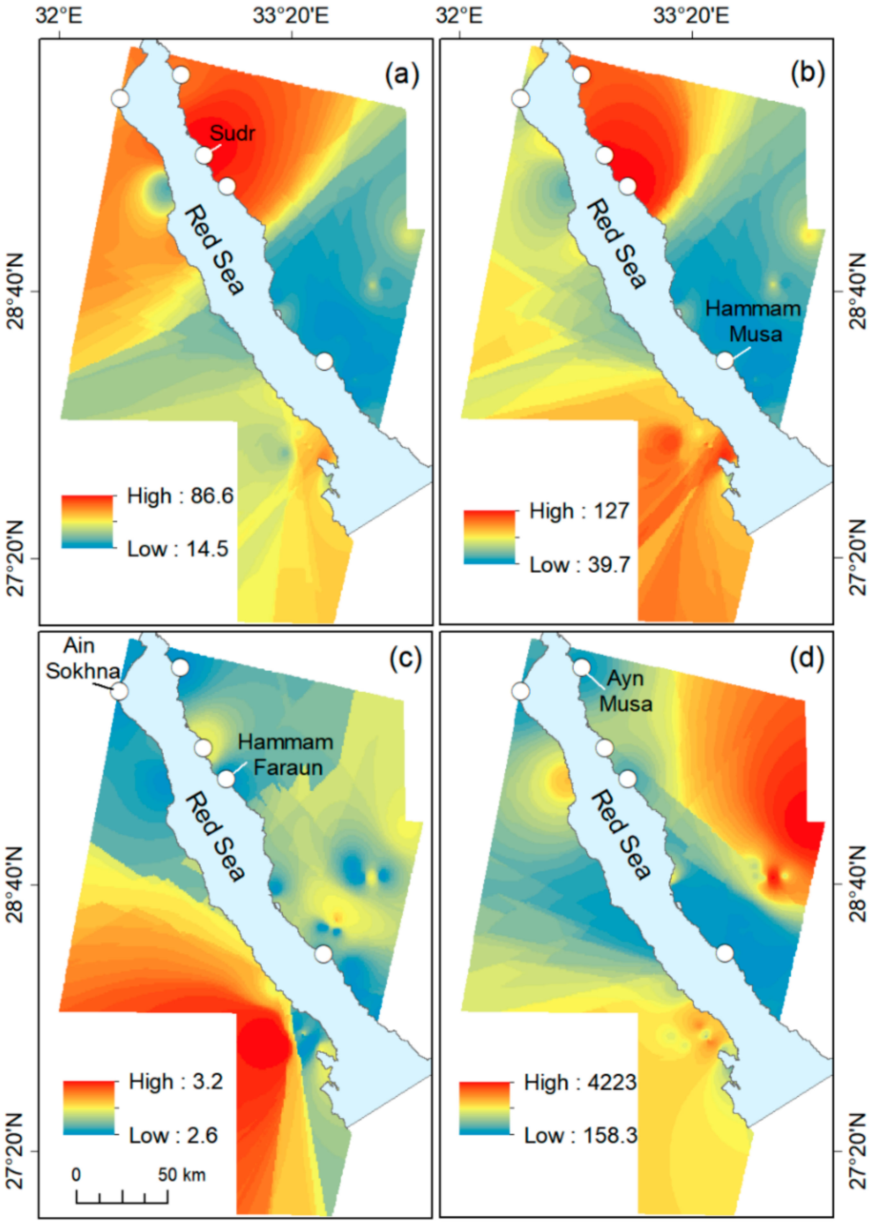

Figure 6. Geothermal thematic layers derived from 37 onshore oil wells. (**a**) Geothermal gradient in °C/km, (**b**) heat flow in m W k^{-1}, (**c**) thermal conductivity in W m^{-1} K^{-1} and (**d**) depth to the crystalline basement in meters. The plotted points show the locations of the thermal springs along the gulf.

3.2. Remote Sensing Data Set and Analysis

3.2.1. Digital Elevation Model (DEM)

The Shuttle Radar Topography Mission (SRTM) (https://earthexplorer.usgs.gov/) was used to deliver information about the topographic properties of the study area. Eight SRTM tiles, at 1 arc second (about 30 m) resolution, were download from the United States Geological Survey (USGS) and mosaicked used in ArcGIS 10.7 (ESRI, Redlands, CA, USA) software to derive relevant variables, including surface elevation, fractures and drainage network density. Surface elevation is a vital element in determining the depth and source to the geothermal reservoir. Such surface terrain is an indicator of the suitability for geothermal prospect and it is one of the principle factors in effecting heat contact of geothermal energy between surface and subsurface. In low elevation areas, it is easy for geothermal energy to rapidly reach the surface and conduct high geothermal recharge. Therefore, geothermal potentiality is expected to be greater in low elevation areas than in those areas of high elevation (Figure 7a).

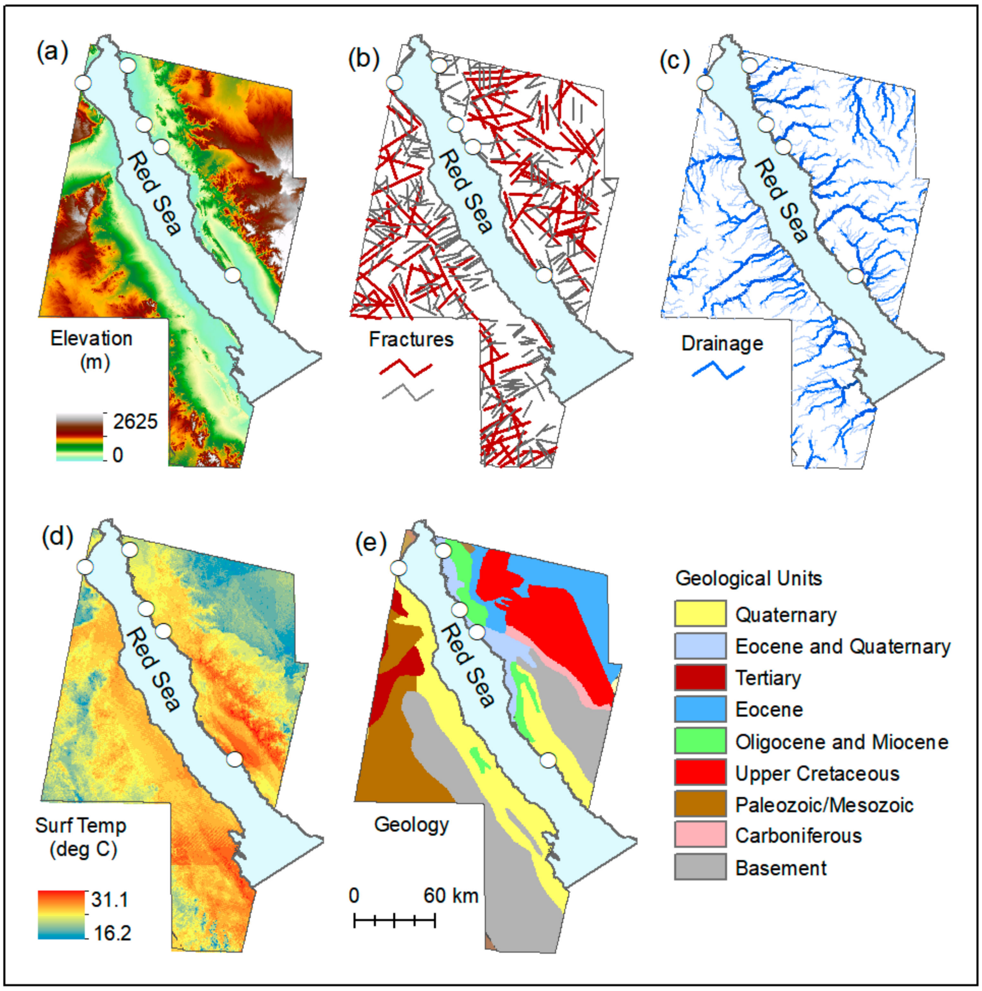

Figure 7. Physiographic and geologic layers extracted from remote sensing thermal infrared and elevation data, and geological unit. (**a**) Surface elevation, (**b**) lineaments (**c**) drainage network, (**d**) nighttime land surface temperature and (**e**) simplified geological units.

Lineaments are defined as mappable linear features of a surface which most likely reflects subsurface structural phenomena [47,48]. Lineaments comprised of fractures, joints and faults is an indication for the subsurface structures that may control the movement, migration, and storage of geothermal energy. Lineaments, particularly of high permeability, play a vital role in the recharging of geothermal energy in the hard rock terrains where geothermal potential is very much higher near dense lineament zones. Therefore, regions of high fracture density can greatly serve as the best horizon for geothermal energy [49]. Lineament density, so-called fault and fracture density (FFD), is a vital variable since many geothermal systems are associated with high densities of faults and fractures [50,51] and productive geothermal wells are associated with permeable faults at depth [52]. Lineaments extraction in this study was performed through visual interpretation and on-screen digitizing of accentuated topography imaged in an eight-direction summed hill-shade generated from the SRTM DEM and very high-resolution imagery on Google Earth Pro. The lineament density, defined as the total length of lineaments per unit area, was constructed for the entire area using the density kernel analysis is ArcGIS (Figure 7b).

Drainage network is one of the important variables for understanding the lithological and geological structures of landform evolution. Drainage courses, particularly those controlled by active structures, can act as conduits where meteoric water gets infiltrate along them into deep hot strata and thus replenish the geothermal local reservoirs. A high drainage density, particularly of those structurally controlled channels, is favorable for geothermal energy availability. The drainage network was delineated based on a procedure by [53], using the widely used 8D flow direction algorithm [54–56]. The stream network was generated using a threshold of 200 cells and matched with those visible in Google Earth Pro imagery for verification. Final stream network was used to derive the drainage density layer, which is defined as the total length of streams per unit area in the associated drainage basin (Figure 7c).

3.2.2. Thermal Infrared Data

Landsat TM data, was obtained from the United States Geological Survey (USGS) and used to map variation in ground surface temperature and potential geothermal anomalies in the study area. Thermal anomalies are locations where land surface temperatures (LST) are warmer than that of the surrounding locations under normal conditions, thus, geothermal potentiality is expected to be greater in spots with warmer surface temperature. Similar to natural hot springs, warm land surface temperature (heated ground) could be among the surface expressions of conductive and convective heat loss from geothermal systems. Thermal Infrared (TIR) remote sensing data can be used to map the spatial distribution and extent of temperature anomalies associated with surface geothermal features such as hot springs and heated ground [57–59]. An early study by [60], using thermal imagery in the region of Long Valley and the Salton Sea, California, detect heated ground overlying faults providing potential indicators of geothermal upwelling zones. Another study by [61], using a stack of Landsat thermal imagery in the Island of Akutan, Alaska, has identified a known field of thermal springs and revealed three new distinct regions with persistent warm surface temperature anomalies providing targets for field investigations.

Cloud-free Landsat Thematic Mapper (TM 4 and 5) nighttime thermal scenes, at 120 m spatial resolution, were acquired between September and November 1989. The nighttime land surface temperature was chosen over the daytime data to eliminate the direct effect of solar heat. Moreover, older Landsat data (1989) was used instead of the present LS data, as in 1989 the ground surface of the study area was more exposed whereas today large segments of the coastal strip are masked by modern developments. All thermal infrared bands (spectral channel 6 covering a spectral window of 10.40–12.50 μm) were radiometrically calibrated in ENVI 5.5.1 software (HARRIS GEOSPATIAL SOLUTIONS, INC, Broomfield, CO, USA) to surface kinetic temperature and converted to degrees Celsius. The TIR calibrated bands were mosaicked to highlight persistent surface temperature anomalies and heated ground overlying large faults as possible indicators of geothermal upwelling zones (Figure 7d).

3.3. Geological Units Layer

Geological rock units play an important role in hosting and transporting the geothermal energy and heat flow from the deep subsurface to the surface. Basement rocks can produce geothermal energy and heat easily from the heat source of the mantle. Sedimentary rocks can also host considerable geothermal reservoirs. The main rock types occurring in the study area consist of basement rocks, Carboniferous, Paleozoic and Mesozoic, Triassic/Jurassic, Upper Cretaceous, Eocene, Oligocene, Miocene and Quaternary rocks. Regions in or near basement rocks, Eocene and Quaternary, Oligocene and Miocene and Carboniferous sediments can be good sources for geothermal energy and thermal conductivity. Likewise, regions along geological contact zones between basement and tertiary rocks, such as the Zeit formation, south Gharib and Belayim formations (Miocene) are favorable for geothermal exploitation. In the present study, the geothermal potentiality is expected to be greater in basement, Miocene, and Carboniferous rocks. Dominant geological rock units in the area, obtained from the Egyptian Geological Survey and Mining Authority (EGSMA) at a scale of 1:100,000, were on-screen digitized in ArcMap (Figure 7e).

3.4. GIS-Based Geothermal Potential Model

The developed GIS-based geothermal potential model can serve as a guide for selection of locations that may merit detailed geothermal resource exploration in the Gulf of Suez area. The produced nine raster layers (geothermal gradient, heat flow, thermal conductivity, depth to basement, surface altitude, fractures density, drainage density, land surface temperature and geological units) where then reclassified on a scale of 1–5, with 5 being most favorable (Figure 8). High geothermal gradient, high heat flow, high thermal conductivity, low depth to basement, high fractures and drainage density, high land surface temperature, low surface elevation and basement rock units received the highest values. The simple additive weight (SAW) technique was applied to these nine intermediate layers to derive the geothermal potential map. More weight was applied to the four derived field data layers (oil wells data) due to their importance as geothermal indicators.

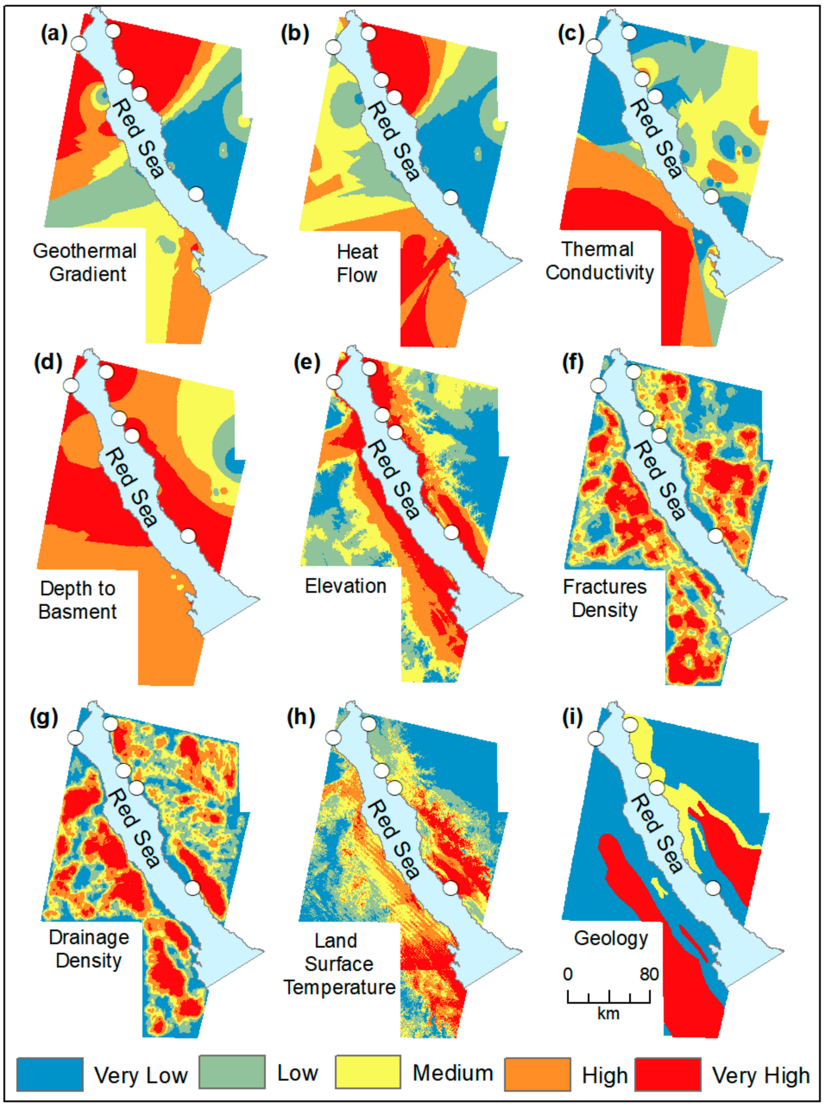

Figure 8. Geothermal potential thematic layers. (**a**) Geothermal gradient, (**b**) heat flow, (**c**) thermal conductivity, (**d**) depth to crystalline basement, (**e**) surface elevation, (**f**) fractures density, (**g**) drainage density, (**h**) nighttime land surface temperature, (**i**) geological units.

4. Results

The corrected BHT using Horner and Gulf of Mexico correction approaches indicated that the study area has a geothermal gradient ranging from 24.9 to 86.66 °C/km, and a heat flow ranging from 31 to

127.2 m W k^{-1}. Additionally, the thermal conductivity was found to be in the range of 2.6–3.2 W m^{-1} k^{-1}, with an amplitude temperature varying from 49.48 °C to 157.8 °C, and an oil window in the range of 66.08–0.5 m. The data revealed also that the maximum geothermal gradients were recorded at Sudr hot spring in addition to five wells including GS-306, RR-89, SB-307, GH-451, and Hammam Faraun with a thermal gradient values of 86.66, 65.4, 51.9, 49.1, 4.8 and 48 °C/km, respectively.

The geothermal gradient and heat flow data were plotted against the depth to basement and thickness of overburden rocks in order to understand their correlations throughout the Gulf of Suez area. Analysis revealed that there is an inverse relationship between geothermal gradient and heat flow with both the depth to basement rocks and load of overburden rocks (Figure 9). Areas with substantial shallow depth to basement and reduced thickness of overburden rocks, such as the northeastern segment of the Gulf of Suez, where the three hot springs of Hammam Faraun, Sudr and Ayn Musa lie, correspond to high geothermal gradient and heat flow. This area has a shallow depth to basement with an average of 450 m and high geothermal gradient, heat flow and thermal conductivity of 58.2 °C/km, 102.24 m W k^{-1}, 2.62 W m^{-1} k^{-1}, respectively. In contrast, areas, such as in Zaafaranna site in the northwest of the Gulf, with a depth of basement of 943 m, have a considerably low geothermal gradient, heat flow and thermal conductivity of 24.28 °C/km, 63.12 m W k^{-1}, 2.60 W m^{-1} k^{-1}, respectively. The geothermal data indicates that the depth to basement rocks generally increases southward in the Gulf of Suez region, however, such depth varies widely (between 158.3 m to 4223 m in some localities), which could be due to the presence of controlling structures related to the Gulf of Suez tectonics. This indicates that the Gulf area is consisted of different faulted blocks forming the uplifted basement and the deep basins, which most likely are of great importance for geothermal exploration and oil production.

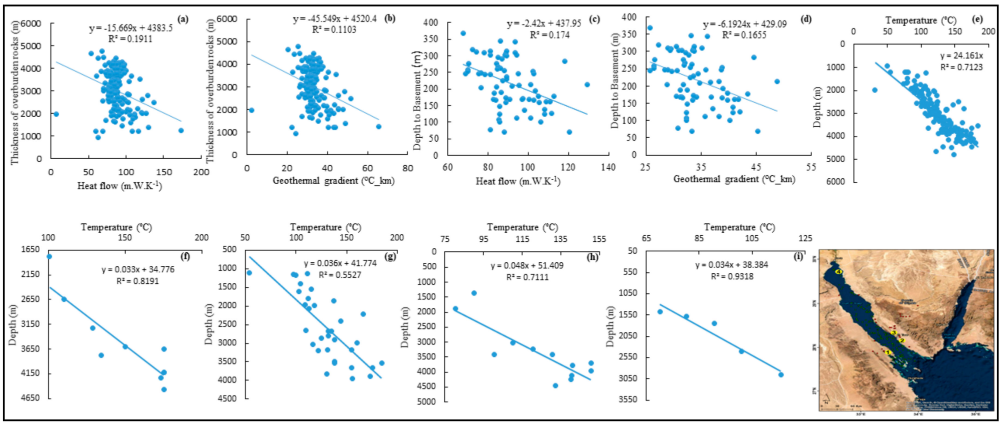

Figure 9. Shows inverse relationship of wells data. (**a**,**b**) Geothermal gradient and heat flow with thickness of overburden rocks, (**c**,**d**) geothermal gradient and heat flow with depth to crystalline basement across the study area. (**e**) Bottom hole temperature (BHT) of 197 oil wells (onshore and offshore) versus depth to basement along the Gulf of Suez region. (**f**,**g**,**h**,**i**) BHT and geothermal gradients four selected wells (Al Amir (**f**), GS (**g**), SB (**h**), and Darag, (**i**) wells marked in yellow on the lower right image). Region with shallow depth and narrow overburden rocks have high geothermal gradient and heat flow.

Potential Locations for Geothermal Exploration

The derived nine raster layers were integrated through the SAW approach, to generate the geothermal potential model (GTP) for the Gulf of Suez area (Figure 10). The GTP, is categorized into four different zones that range from low to very high geothermal potential. Based on the model, the northeastern and southwestern areas of the Gulf of Suez were predicted to hold very high geothermal potential in the area under investigation.

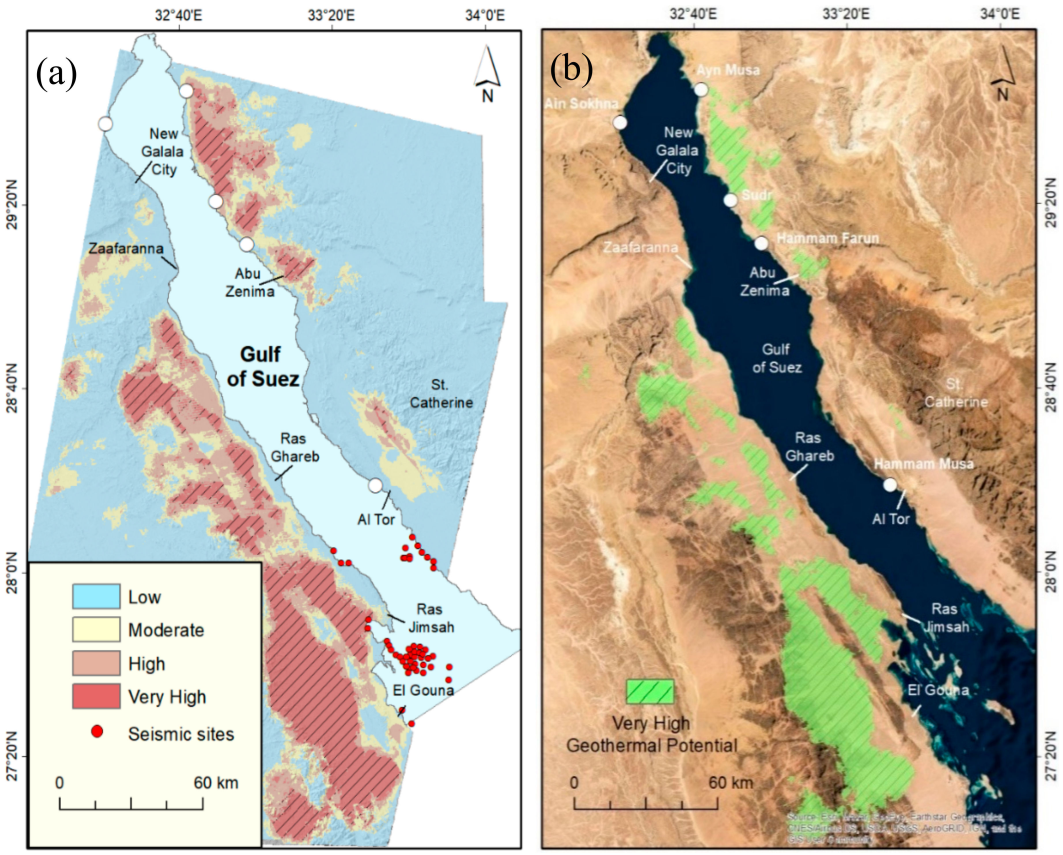

Figure 10. (**a**) Geothermal potential prospect map along the Gulf of Suez region. (**b**) Very high geothermal potential zone, highlighted in stripped green color, is superimposed on a satellite image (ArcGIS Basemap) of the study region. Both the northeastern and southwestern areas of the Gulf of Suez are predicted to hold very high geothermal potential.

The first area of very high geothermal potential lies in the northeastern part of the Gulf of Suez and extends from Ayn Musa north to Abu Zenima City south. This particular location, which covers an area of 597 km^2, is characterized by superficial thermal manifestations represented by a cluster of hot springs. Three known hot springs lie within this zone (Hammam Faraun, Sudr and Ayn Musa) with Sudr and Hammam Faraun represent the hottest spring in Egypt with a high heat flow of 110.23 and 127.2 m W k^{-1}, respectively, about 3 times the normal values in the eastern part of Egypt [15]. Data analysis revealed that this area has high fractures density and structurally controlled stream network, which are principle factors in effecting heat contact of geothermal energy between surface and subsurface. A numerical model of the geothermal system developed at this site indicated that Hammam Faraun geothermal resource originates due to its tectonic position and high heat flow as well as the deep circulation of groundwater in the structurally controlled subsurface reservoirs [62]. Based on stable isotopes of ^{18}O and Deuterium of thermal water samples collected from the three different hot springs in the area, it was proposed that their recharge may be due to the mixing and circulation of the Gulf of Suez water with the meteoric water that comes from regions of high altitude via sporadic rainfall-surface runoff events or that enclosed the geothermal reservoir [63].

The shallow depth to basement rocks of 158.3 m, combined with low surface topography highlight this area as a promising geothermal site. In such low topographic area, geothermal energy can rapidly reach the surface and conduct high geothermal recharge. Moreover, this area is characterized by tectonic uplift of hot basement rocks and is made up of sedimentary rocks, which contain hot underground water heated by the underneath bedrocks. Basement rocks (mainly gneisses and younger granites), the main source of heat, as well as Paleozoic sedimentary cover (mainly Carboniferous sediments), which contain organic layers (coal seams) [64] and rich in radioactive elements (trace element) like U, Th, Rb, and Sr particularly in Um Bogma formation, could all be good indicators of high geothermal energy.

The second area of very high geothermal potential lies at the southwestern part of the Gulf of Suez [65], which extents between the town of Zaafarana north and Hurghada City south. This zone covers a large extent of 4019 km^2 and includes Ras Ghareb, Gabal El-Zeit and El-Gouna areas. It is marked by high geothermal gradient, heat flow and thermal conductivity with maximum values of 32.972 °C/km, 88.34 m W k^{-1} and 2.68 W m^{-1} K^{-1}, respectively. The site is identified by increased thickness of Nubian sandstone and Limestone, which considered as a good reservoir for the geothermal energy due to its high petrophysical properties (e.g., porosity and permeability). Moreover, the site is characterized by high fractures density, which increases the chance for the geothermal energy to spread and diffuse easily in a large amount, and thus, suggests a region of a high tectonic activity and rejuvenation. Seismic data of the Gulf of Suez (obtained from [66]), revealed the proximity of the southwestern area to a cluster of microearthquakes of high magnitude and frequency, which further support the high geothermal potential at this site. Moreover, this area has a notable drainage density (mostly structurally controlled), which most likely enhances the infiltration of meteoric water and facilitates rapid replenishments of the local geothermal reservoirs.

Both the northeastern and southwestern sites have high rock porosity, which serves as an important factor that can increase the spreading of the geothermal heat. The stratigraphic successions of the northeastern zone, around the two hot springs of Hammam Faraun and Ayn Musa were mapped (modified after [29,67]) to determine the thickness and geological formation properties of the underneath geothermal reservoirs (Figure 11). Analysis of these successions showed that the thickness of the sandstone and limestone rocks in Hammam Faraun and Ayn Musa reaches 500 m and 400 m, respectively. The existence of Miocene deposits with high porosities of 11–24% [68] in this particular area along with the southwestern area of the Gulf (for instant, the Rudies, Kareem, Hammam Faraun, Belayim and South Gharib formations) proposes the presence of a sizeable geothermal reservoirs. The research of [69] indicated that these Miocene rocks, particularly in Zeit, South Gharib and Belayim formations, along with the basement rocks exhibit the highest estimated thermal conductivity values of W/m/K (~3–3.5). Rocks with high porosity have high heat conduction property which fasten the heat flow through the rock.

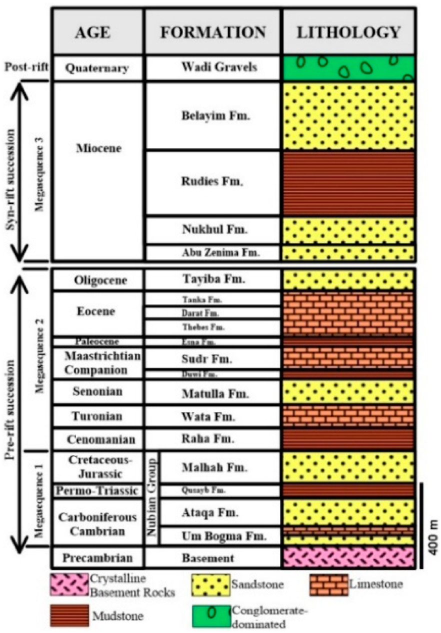

Figure 11. Schematic diagrams show the stratigraphic succession in the Hammam Faraun (means Pharaoh's Bath) hot spring, modified after [67].

The IDW interpolated geothermal layers (Figure 12), derived from the corrected 160 offshore wells logging data along the Gulf of Suez, were superimposed on the GTP map for model validation. Analysis revealed the presence of relatively shallow depth to basement with high geothermal gradient and heat flow, with an average of 1350 m, 42 °C/km, and 110 m W k^{-1}, respectively, at the norther and southwestern segments of the Gulf of Suez. These segments lie right next to the two proposed very high geothermal potential areas (Figure 12), validating the outcomes of the adopted model.

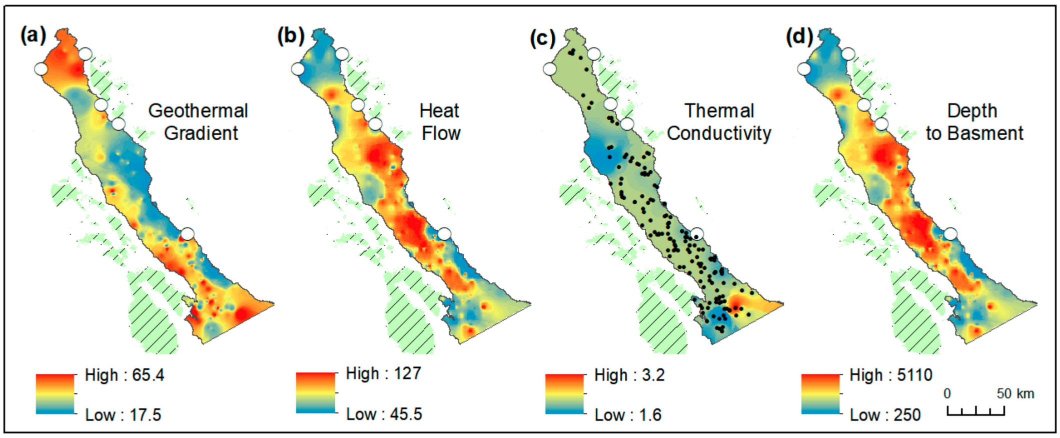

Figure 12. Shows the offshore geothermal parameters and their distributions along the Gulf of Suez. (**a**) geothermal gradient, (**b**) heat flow, (**c**) thermal conductivity overlaid by locations of offshore oil wells, and (**d**) depth to the crystalline basement. As illustrated, there are a general clustering of high geothermal gradient, heat flow and thermal conductivity with shallow depth to basement in the northern and southwestern segments of the Gulf of Suez.

5. Discussion

With Egypt's rapid population growth, reaching 102.3 million people in the year 2020, demand continues to grow for new energy resources. Such energy demand is likely to rise even more with the completion and full operation of the new Grand Ethiopian Dam (also known as El-Nahda Dam) on the Blue Nile (the first phase of the reservoir's filling was completed on July 2020). Once completed, this massive hydropower dam will be able to hold 74 billion m^3 of water and produce 6000 MW for Ethiopia [70], while reducing Egypt's hydroelectric power generation by at least 7% during wet years [71]. This mega dam is expected to have devastating consequences on Egypt's water supply and electricity generation during prolonged periods of drought. Today, about 94% of the nations' energy needs are supplied by petroleum products (53% and 41% from oil and natural gas, respectively), while the remaining energy fraction of 6% is provided through hydropower and coal. Although, the presence of many natural hot springs and thermal wells across the Red Sea region, indicating potential geothermal resources, power generation from geothermal plants has not yet established in Egypt.

The two locations identified by the present work are suggested to be of high potential for geothermal energy exploration in the Gulf of Suez region. Although, no estimation was made for the whole geothermal system in Egypt, energy approximations were made for the area of Hammam Faraun due to its unique geothermal characteristics. Through geothermal analysis and numerical simulation, [72,73] have estimated a geothermal production of 12.4 MWt and 19.8 MWt at Hammam Faraun, which considered to be economically appropriate for exploitation and construction of a small binary power plant for electricity production.

Many areas around the world, with natural hot springs and thermal wells, similar to those in the Gulf of Suez region in Egypt, are heavily exploited for geothermal energy. For example, there are 3676 MW of geothermal power plants in operation in the United States alone and several other countries, such as Indonesia (1948 MW), Philippines (1868 MW) and New Zealand (1005 MW) are using geothermal power as a significant share to their energy mix [74]. In Africa, a number of countries in the vicinity of the East African Rift area, such as Tanzania, Ethiopia, Uganda, Rwanda, Djibouti and Eritrea, have recently undertaken preliminary exploration for geothermal potential. Today, nearly 40% of Kenya's electricity is generated from geothermal source, making this nation the largest geothermal energy producer in Africa with an estimated value of 630 MW [75]. It is expected that the global geothermal market achieves 32 GW by the early 2030 s, if all nations follow through on their geothermal power development goals [76]. About 50% of this geothermal market could be provided by Africa alone. Africa's untapped geothermal energy potential is estimated to be 15 GW, which if exploited, could alter the economies and rate of development of many African countries [77]. Egypt's geothermal potential along the Gulf of Suez can contribute considerably to this number.

6. Conclusions

Despite the fact that Egypt is not among those nations that characterized by ample Cenozoic igneous activity, its position in the northeastern side of the African plate strongly proposes that the country might have unexplored geothermal resources, particularly along its eastern territory. Field data, obtained from 197 offshore and onshore deep oil wells along the Gulf of Suez, were used in this study. The corrected well logging data along with the geological and remote sensing thermal infrared and digital elevation tiles were processed to generate the relevant geothermal and physiographic variables for the area under investigation. Nine raster layers, including geothermal gradient, heat flow, thermal conductivity and depth to crystalline basement, elevation, lineaments density, land surface temperature, drainage density, major lithological units were combined in GIS to model the geothermal potential map for the Gulf of Suez region. The model identified the northeastern and the southwestern areas of the Gulf as equally two sites of very high geothermal potential, thus possible locations for future geothermal exploration. These two sites show remarkably high geothermal gradient, heat flow, shallow depth to crystalline basement, low surface elevation, high fractures and drainage density and most importantly high rock porosity, which all serves as vital factors in increasing the spreading of the geothermal heat and aid the geothermal energy to rapidly reach the surface. The presence of high geothermal gradient and heat flow, along with shallow depth to basement, in the offshore zone of the Gulf, right next to the two proposed sites support the result derived by the adopted geospatial model. The method implemented in this study enables a rapid identification of promising geothermal hotspots and provide vital information for future geothermal exploration planning purposes in Egypt.

Author Contributions: E.G., developed the research framework, designed the research question, supervised the entire project (methodology, analysis, and interpretation), created all the figures and wrote, reviewed, and edited the manuscript; A.S.F., performed the work, collected the data, conducted the methods, data analysis, and helped in preparing all the figures and writing the manuscript; M.A.N., developed the research framework for the geological section, provided inputs for geological part, reviewed, and helped in writing the geological part; A.M., helped in data collection and contributed to the well and natural spring dataset. All authors have read and agreed to the published version of the manuscript.

Funding: This research was fully funded by the Egyptian Government. Travel expenses and publication fee were provided through a grant to E. Ghoneim funded by the Embassy of the Arab Republic of Egypt, Cultural and Educational Bureau, Washington, DC, USA.

Acknowledgments: This research was conducted at the UNCW Space and Drone Remote Sensing Lab (SDRS). Thanks to the Egyptian General Petroleum Corporation (EGPC) for providing the oil well data. The authors would like to express their appreciation for Dr. Mohamed Abd El Zaher, at the National Research Institute of Astronomy and Geophysics (NRIAG), and Prof. Essam Aboud, at the Geohazards Research Center, King Abdul-Aziz University, Saudi Arabia, for helping in the well data collection. We thank the anonymous reviewers for their thoughtful comments on this paper.

Conflicts of Interest: The authors declare no conflict of interest.

References

1. Perston, M.; Croker, A. Renewable Energy in Egypt. Hydro, Solar and Wind. Norton Rose Fulbright. 2013. Available online: http://www.nortonrosefulbright.com (accessed on 1 July 2017).
2. Girdler, R.W.; Styles, P. Seafloor spreading in the western Gulf of Aden. *J. Nat.* **1978**, *271*, 615–657. [CrossRef]
3. Bosworth, W.; Huchon, P.; Mc Clay, K. The Red Sea and Gulf of Aden Basins. *J. Afr. Earth Sci.* **2005**, *43*, 334–378. [CrossRef]
4. Wolfenden, E.; Ebinger, C.; Yirgu, G.; Renne, P.R.; Kelley, S.P. *Evolution of a Volcanic Rifted Margin*; GSA Bull: Southern Red Sea, Ethiopia, 2005; Volume 117, pp. 846–864.
5. Chandrasekharam, D.; Lashin, A.; Al Arifi, N.; Al Bassam, A.A.; Varun, C. Evolution of geothermal systems around the Red Sea. *J. Environ. Earth Sci.* **2015**, *73*, 4215–4236. [CrossRef]
6. Chandrasekharam, D.; Lashin, A.; Al Arifi, N.; Al Bassam, A.; Varun, C.; Singh, H.K. Geothermal energy potential of Eastern Desert region. *Egypt. J. Environ. Earth Sci.* **2016**. [CrossRef]
7. El Shazly, E.M.; Saleeb Roufaiel, G.S. Metasomatism of Miocene sediments in St. John's Island and its bearing on the history of the Red Sea. *Egypt J. Geol.* **1977**, *21*, 103–108.
8. Bosworth, W.; Tavian, M. Late quaternary reorientation of stress field and extension direction in the southern Gulf of Suez, Egypt: Evidence from uplifted coral terraces, mesoscopic fault arrays and bore-hole breakouts. *J. Tecton.* **1996**, *15*, 791–802. [CrossRef]
9. Siedner, G. K–Ar chronology of Cenozoic volcanic from northern Israel and Sinai. Fortschr. *J. Miner.* **1973**, *50*, 129–130.
10. Meneisy, M.Y.; Kreuzer, H. Potassium-argon ages of Egyptian basaltic rocks. *J. Geol. Jahrb.* **1974**, *D9*, 21–31.
11. Chandrasekharam, D.; Bundschuh, J. *Low Enthalpy Geothermal Resources for Power Generation*; Taylor and Francis Publisher: Abingdon-on-Thames, UK, 2008; p. 169.
12. Boulos, F. Some Aspects of the Geophysical Regime of Egypt in Relation to Heat Flow, Groundwater and Micro Earthquakes. In *The Geology of Egypt*; Said, R., Ed.; Balkema: Rotterdam, The Netherlands, 1990; pp. 407–438.
13. McKenzie, D.P.; Davies, D.; Molnar, P. Plate tectonics of the Red Sea and East Africa. *J. Nat.* **1970**, *226*, 243–248. [CrossRef]
14. Morgan, P.; Boulo, K.; Henni, S.F.; Eleri, A.A.; El-Saye, A.A.; Bast, N.Z.; Mele, Y.S. Heat flow in Eastern Egypt: The thermal signature of a continental breakup. *J. Geo Dynam* **1985**, *4*, 107–131. [CrossRef]
15. Morgan, P.; Swanberg, C.A. Heat flow and the geothermal potential of Egypt. *Geotherm. Geotherm. Energy Birkhäuser Basel* **1979**, *117*, 213–226.
16. El-Nouby, M.R. Distribution of Potassium Deposits at Ras El Bohae Area, Gulf of Suez. Master's Thesis, Al-Azhar University, Cairo, Egypt, 1990.
17. Saleh, S.; Jahr, T.; Jentzsch, G.; Saleh, A.; Ashour, N.M.A. Crustal evaluation of the northern Red Sea rift and Gulf of Suez, Egypt from geophysical data: 3-dimensional modelling. *J. Afr. Earth Sci.* **2006**, *45*, 257–278. [CrossRef]
18. Lashin, A. Review of the Geothermal Resources of Egypt: 2015–2020. In Proceedings of the World Geothermal Congress 2020, Reykjavik, Iceland, 26 April–2 May 2020.
19. Morgan, P.; Black'well, D.D.; Fanis, T.G.; Boulos, F.K.; Salib, P.G. Preliminary temperature gradient and heat flow values for northern Egypt and the Gulf of Suez from oil well data. In Proceedings of the International Congress on Thermal Waters, Geothermal Energy and Volcanism of Mediterranean Area, Athens, Greece, 5–10 October 1976; pp. 424–438.
20. Colletta, B.; Le Quellec, P.; Letouzey, J.; Moretti, I. Longitudinal evolution of the Suez rift structure (Egypt). *J. Tectonophys.* **1988**, *153*, 221–233. [CrossRef]
21. Bayer, H.J.; El Isa, Z.; Hotzl, H.; Mechie, J.; Prodehl, C.; Saffarini, G. Large tectonic and lithospheric structures of the Red Sea region. *J. Afr. Earth Sci.* **1989**, *8*, 565–587. [CrossRef]
22. Camp, V.E.; Roobol, M.J. Upwelling Asthenosphere beneath Western Arabia and Its Regional Implications. *J. Geophy. Res.* **1992**, *97*, 15255–15271. [CrossRef]
23. Bosworth, W.; Mc Clay, K. Structural and stratigraphic evolution of the Gulf of Suez Rift, Egypt: A synthesis. In *Peri-Tethys Memoir 6: Peri-Tethyan Rift/Wrench Basins and Passive Margins*; Ziegler, P.A., Cavazza, W., Robertson, A.H.F., Crasquin-Soieau, S., Eds.; Museum National d'Histoire Naturelle: Paris, France, 2001; Volume 186, pp. 567–606. ISBN 2-85653-528-3.

24. Omara, S. An early Cambrian outcrop in southwestern Sinai, Egypt. *N. JP. J. Geol. Palaeontol.* **1972**, *5*, 306–314.
25. EGSMA (Egyptian Geological Survey and Mining Authority). *Geologic Map Sinai, Egypt, (Scale 1:100,000)*; Upper Egypt Governorates: Cairo, Egypt, 1993.
26. Moustafa, A.; Khalil, M.H. Rejuvenation of the eastern Mediterranean Passive continental margin in northern and central Sinai: Newdat from the Themed Fault. *J. Geol Mag* **1993**, *131*, 435–448. [CrossRef]
27. Kora, M. An introduction to the stratigraphy of Egypt. In *Lecture Notes*; Geology Department Mansoura University: Mansoura, Egypt, 1995; p. 116.
28. Moustafa, A.M. Block faulting in the Gulf of Suez. In Proceeding of 5th Egyptian General Petroleum Corporation Exploration Seminar, Cairo, Egypt, November 1976; p. 35.
29. Egyptian Geological Survey and Mining Authority (EGSMA). *Flash Floods of November 1994*; Upper Egypt Governorates: Cairo, Egypt, 1994. (in Arabic)
30. Abdel-Gawad, M. The Gulf of Suez: A brief review of stratigraphy and structure. *Phil. Trans. Roy. Soc. Lond.* **1970**, *267*, 41–48.
31. Tawfik, N.; Harwood, C.; Deighton, I. The Miocene, Rudeis and Kareem formations of the Gulf of Suez. Aspects of Sedimentology and Geohistory. In Proceedings of the 11th Petroleum Exploration and Production Conference, Cairn, Egypt, 7–10 November 1992; pp. 84–113.
32. Said, R. Cretaceous Paleogeographic maps. In *The Geology of Egypt*; Balkema: Rotterdam, The Netherlands, 1990; pp. 439–449.
33. Meshref, M.W. Tectonic framework of Egypt. In *Geology of Egypt*; Balkema Publisher: Rotterdam, The Netherlands, 1990.
34. Geschet, D.B.; Verdin, K.L.; Greenlee, S.K. New land surface digital elevation model covers the Earth. *J. Eos Trans. AGU* **1999**, *80*, 69–70. [CrossRef]
35. Kaiser, M.F.; Ahmed, S.G. Optimal thermal water locations along the Gulf of Suez coastal zones. *Egypt. J. Renew. Energy* **2013**, *55*, 374–379. [CrossRef]
36. Horner, R.D. Pressure build-up in wells. In Proceedings of the Third World Petroleum Congress, The Hague, The Netherlands, 28 May–6 June 1951; pp. 34–316.
37. Waples, D.W.; Pacheco, J.; Vera, A.A. Method for correcting log-derived temperatures in deep wells, calibrated in the Gulf of Mexico. *J. Pet. Geosci.* **2004**, *10*, 239–245. [CrossRef]
38. Lachenbruch, A.H.; Brewer, M.C. *Dissipation of the Temperature Effect of Drilling a Well in Arctic Alaska*; US Government Printing Office: Washington, DC, USA, 1959; Volume 1083-C, pp. 73–109.
39. Ribeiro, F.B.; Hamza, V.M. Stabilization of bottom holes temperature in the presence of formation fluid flows. *J. Geophys.* **1986**, *51*, 410–413. [CrossRef]
40. Shen, P.Y.; Beck, A.E. Stabilization of bottom hole temperature with circulation time and fluid flow, Geophysics. *J. Roy. Aston. Soc.* **1986**, *86*, 63–90. [CrossRef]
41. Dowdle, W.L.; Cobb, W.M. Static formation temperature from well logs, an empirical method. *J. Petrol. Technol.* **1975**, *27*, 1326–1330. [CrossRef]
42. Middleton, M.F. A model for bottom-hole temperature stabilization. *J. Geophys.* **1979**, *44*, 1458–1462. [CrossRef]
43. Luheshi, M.N. Estimation of formation temperatures from borehole measurements. *J. Geophysics. Roy. Aston. Soc.* **1983**, *74*, 747–776.
44. Morgan, P.; Boulos, K.; Swanberg, C.A. Regional geothermal exploration in Egypt. *J. Eaeg* **1983**, *31*, 361–376. [CrossRef]
45. Lashin, A.; Al Arifi, N. Some Aspects of the Geothermal Potential of Egypt. Case Study: Gulf of Suez-Egypt. In Proceedings of the World geothermal Congress, Bali, Indonesia, 25–29 April 2010.
46. Prensky, S. Temperature measurements in boreholes: An overview of engineering and scientific applications. *J. Log Anal.* **1992**, *33*, 313–333.
47. O'Leary, D.W.; Friedman, J.D.; Pohn, H.A. Lineament, linear, lineation: Some proposed new standards for old terms. *J. Geol. Soc. Am. Bull.* **1976**, *87*, 1463–1469. [CrossRef]
48. Abrams, W.; Ghoneim, E.; Shewa, R.; La Maskina, T.; Al-Bloushib, K.; Hussein, S.; Abu Bakr, M.; Al-Mullad, E.; Al-Aware, M.; El-Baz, F. Delineation of groundwater potential (GWP) in the northern United Arab Emirates and Oman using geospatial technologies in conjunction with Simple Additive Weight (SAW), Analytical Hierarchy Process (AHP), and Probabilistic Frequency Ratio (PFR) techniques. *J. Arid Env.* **2018**, *157*, 77–96. [CrossRef]

49. Hanano, M. Two different roles of fractures in geothermal development. In Proceedings of the World Geothermal Congress, Kyushu–Tohoku, Morioka, Japan, 28 May–10 June 2000; pp. 2597–2602.
50. Les Landes, A.; Guillon, T.; Borie, M.P.; Blaisonneau, A.; Rachez, X.; Gentier, S. Locating Geothermal Resources: Insights from 3D Stress and Flow Models at the Upper Rhine Graben Scale. *Geomech. Fluid Flow Geotherm. Syst.* **2019**, *2019*, 8494539. [CrossRef]
51. Wallis, I.C.; McNamara, D.; Rowland, J.V.; Massiot, C. The nature of fracture permeability in the basement grey-wacke at Kawerau Geothermal Field, New Zealand. In *Thirty-Seventh Workshop on Geothermal Reservoir Engineering*; Stanford University: Stanford, CA, USA, 2012.
52. Grindley, G.W. *The Geology, Structure and Exploitation of the Wairakei Geothermal Field, Taupo, New Zealand*; Bulletin No. 75; New Zealand Geological Survey: Wellington, New Zealand, 1965; 131p.
53. Jenson, S.K.; Domingue, J.O. Extracting topographic structure from digital elevation data for geographic information system analysis. *Photogramm Eng. Remote Sens.* **1988**, *54*, 1593–1600.
54. Maidment, D.R. *Handbook of Hydrology.*, 1st ed.; McGraw-Hill: New York, NY, USA, 1993; 1424p.
55. Ghoneim, E.; Benedetti, M.; El-Baz, F. An integrated remote sensing and GIS analysis of the Kufrah Paleoriver, eastern Sahara, Libya. *J. Geomorphol.* **2012**, *139*, 242–257. [CrossRef]
56. Ghoneim, E. Rimaal: A Sand Buried Structure of Possible Impact Origin in the Sahara: Optical and Radar Remote Sensing Investigation. *J. Remote Sens.* **2018**, *10*, 880. [CrossRef]
57. Haselwimmer, C.; Prakash, A.; Holdmann, G. Quantifying the heat flux and outflow rate of hot springs using airborne thermal imagery: Case study from Pilgrim Hot Springs, Alaska. *J. Remote Sens. Environ.* **2013**, *136*, 37–46. [CrossRef]
58. Lago Gonzalez, D.; Rodriguez-Gonzalez, P. Detection of geothermal potential zones using remote sensing techniques. *J. Remote Sens.* **2019**, *11*, 2403. [CrossRef]
59. Hewson, R.; Mshiu, E.; Hecker, C.; Van der Werff, H.; Van Ruitenbeek, F.; Alkema, D.; Van der Meer, F. The application of day and nighttime ASTER satellite imagery for geothermal and mineral mapping in East Africa. *Int. J. Appl. Earth Obs. Geoinf.* **2020**, *85*, 101991. [CrossRef]
60. Hodder, D.T. Application of remote sensing to geothermal prospecting. *J. Geotherm.* **1970**, *2*, 368–380. [CrossRef]
61. Kienholz, C.; Prakash, A. Geothermal exploration in Akutan, Alaska, using multitemporal thermal infrared images. In Proceedings of the American Geophysical Union, Fall Meeting, San Francisco, CA, USA, 14–18 December 2009.
62. Abdel Zaher, M.; Saibi, H.; Nishijima, J.; Mesbah, H.; Fujimitsu, Y.; Ehara, S. Exploration and assessment of the geothermal resources in the Hammam Faraun hot spring, Sinai Peninsula. *Egypt. J. Asian Earth Sci.* **2011**, *45*, 256–267. [CrossRef]
63. Abdel Zaher, M.; Saibi, H.; Ehara, S. Geochemical and stable isotopic studies of Gulf of Suez's hot springs, Egypt. *Chin. J. Geochem.* **2012**, *1*, 120–127. [CrossRef]
64. Abdel Zaher, M.; El Nuby, M.; Ghamry, E.; Mansour, K.H.; Saadi, M.N.; Heba, A. Geothermal studies in oilfield districts of Eastern Margin of the Gulf of Suez. *Egypt. J. Nriag J. Astron. Geophys.* **2014**, *3*, 62–69. [CrossRef]
65. Noweir, M.A.; FAHIL, A.S.; Ghoneim, E.; Masoud, A. Integration and analysis of well logging and remote sensing data for exploring new potential geothermal sites along the Gulf of Suez, Egypt. In Proceedings of the GSA, Joint 69th Annual Southeastern/55th Annual Northeastern Section Meeting, Reston, VA, USA, 20–22 March 2020.
66. Daggett, P.; Morgan, P.; Boulos, F.K.; Hennin, S.F.; El-Sherif, A.A.; El Sayed, A.A.; Basta, N.Z.; Melek, Y.S. Seiosmicity and active tectonics of the Egyptian Red Sea Margin and the northern Red Sea. *J. Tectonophys.* **1986**, *125*, 313–324. [CrossRef]
67. Jackson, C.A.L.; Gawthorpe, R.L.; Sharp, I.R. Growth and linkage of the East Tanka fault zone; structural style and syn-rift stratigraphic response. *J. Geo. Soc. Lond.* **2002**, *159*, 175–187. [CrossRef]
68. Shimron, A.E. Evolution of the Kid Group, southeast Sinai Peninsula: Thrusts, melanges, and implications for accretionary tectonics during the Late Proterozoic of the Arabian-Nubian shield. *Geology* **1984**, *12*, 242–247. [CrossRef]
69. Lashin, A. Geothermal Resources of Egypt: Country Update. In Proceedings of the World Geothermal Congress, Melbourne, Australia, 19–25 April 2015.

70. Tesfa, B. Benefit of Grand Ethiopian Renaissance Dam Project (GERDP) for Sudan and Egypt. In *EIPSA Communicating Article: Energy, Water, Environment & Economic*; University of Huddersfield Repository: Huddersfield, UK, 2013.
71. Mulat, G.; Moges, A. Assessment of the Impact of the Grand Ethiopian Renaissance Dam on the Performance of the High Aswan Dam. *J. Water Resour. Prot.* **2014**, *6*, 583–598. [CrossRef]
72. Abdel Zaher, M.; Nishijima, J.; Fujimitsu, Y.; Ehara, S. Assessment of Low-Temperature Geothermal Resource of Hammam Faraun Hot Spring, Sinai Peninsula, Egypt. In Proceedings of the 36th Workshop on Geothermal Reservoir Engineering Stanford University, Stanford, CA, USA, 31 January–2 February2011.
73. Lashin, A. A Preliminary Study on the Potential of the Geothermal Resources around the Gulf of Suez, Egypt. *Arab. J. Geosci.* **2013**, *6*, 2807–2828. [CrossRef]
74. Available online: https://www.thinkgeoenergy.com (accessed on 13 January 2019).
75. Dutiro, L. The Power of the unknown: Geothermal energy in Zimbabwe. The Chronicle published 11 June 2019. Available online: https://www.chronicle.co.zw/the-power-of-the-unknown-geothermal-energy-in-zimbabwe/ (accessed on 21 June 2020).
76. Annual, U.S. & Global Geothermal Power Production Report March 2016. Available online: https://geothermal.org/Policy_Committee/Documents/2016_Annual_US_Global_Geothermal_Power_Production.pdf (accessed on 20 June 2020).
77. Hafner, M. *Energy in Africa*; Springer Briefs Energy; Springer: Cham, Switzerland, 2018; Volume 47.